Topological states of thermoelectric Yb-filled skutterudites

Hong-Jie Pang [1,2] Hao Yu,[3,2] Wei-Jian Li,[4,2] Liu-Cheng Chen,[3,2] Peng-Fei Qiu,[5] Qing Peng [3,6] and Xiao-Jia Chen[3,2,*]

[1]*Key Laboratory of Artificial Structures and Quantum Control (Ministry of Education), School of Physics and Astronomy,*
Shanghai Jiao Tong University, Shanghai 200240, China
[2]*Center for High Pressure Science and Technology Advanced Research, Shanghai 201203, China*
[3]*School of Science, Harbin Institute of Technology, Shenzhen 518055, China*
[4]*National Laboratory of Solid State Microstructures and School of Physics, Nanjing University, Nanjing 210093, China*
[5]*State Key Laboratory of High Performance Ceramics and Superfine Microstructure, Shanghai Institute of Ceramics,*
Chinese Academy of Sciences, Shanghai 200050, China
[6]*State Key Laboratory of Nonlinear Mechanics, Institute of Mechanics, Chinese Academy of Sciences, Beijing 100190, China*

The effects of topological states on the thermoelectric performance of a highly efficient thermoelectric Yb-filled $CoSb_3$ skutterudite are investigated through combined *ab initio* calculations and electrical transport measurements. The nontrivial topological states are revealed by *ab initio* calculations and inferred from anomalous Hall conductivity and magnetoresistance. The linear bands associated with the topological states lead to low single-band effective mass and high carrier mobility, and consequently high power factor. Furthermore, the additional band minima due to filling the voids with Yb atoms raise the valley degeneracy, which favors the density-of-states effective mass and thus the Seebeck coefficient but scarcely changing the carrier mobility. These effects together contribute to the high power factor of Yb-filled $CoSb_3$ skutterudite. Our results show that topological states play a crucial role in improving the performance of thermoelectric materials.

I. INTRODUCTION

Thermoelectric materials are promising sustainable energy materials due to their ability to convert waste heat into electricity. The conversion efficiency is determined by the dimensionless figure of merit, defined as $zT = S^2\sigma T/\kappa$, where S is the Seebeck coefficient, σ is the electrical conductivity, T is the absolute temperature, and κ is the thermal conductivity consisting of lattice thermal conductivity (κ_l) and electronic thermal conductivity (κ_e) [1]. An excellent thermoelectric material should simultaneously possess large S and high σ to reach an optimal power factor (PF $= S^2\sigma$) and low κ. Nevertheless, the interdependencies of these parameters make it difficult to optimize one parameter without affecting the others. Band engineering and nanostructuring are currently typical ways to optimize PF and κ_l, respectively, by sacrificing other transport parameters [2–5]. Topological insulators are bulk insulating but have topologically protected metallic surface states, leading to notably high carrier mobility (μ) and σ values [6]. Many topological insulators have been known as good thermoelectric materials [7], such as Bi_2Te_3, Bi_2Se_3, and their alloy $Bi_2Te_{3-x}Se_x$ [1,6,8–11]. The nontrivial topological states may have the potential to enhance thermoelectric performance [12–14].

Filled skutterudite based on $CoSb_3$ exhibits great promising thermoelectric performance due to its unique structure [15,16]. Filling the voids of $CoSb_3$ with atoms results in

a significant reduction of κ without deteriorating PF. As a result, high zT values ($zT=1.4-1.7$) have been achieved in n-type single- and multielement-filled skutterudites [17–23]. The mechanism behind the low κ_l in these materials has been extensively studied [15,16,24–28]. However, research on the filling effect on the high PF of filled skutterudites is comparatively scarce. The carrier concentration (n) has been optimized by filling the voids with atoms. Generally, an increase in σ leads to a prominent decrease in S due to their inverse relationship [1]. However, previous studies have shown that filling $CoSb_3$ with Yb atoms results in a significant increase in σ but only a slight decrease in S [17–23]. Understanding the mechanism behind this behavior is crucial to achieve high-performance thermoelectric materials.

Several possible mechanisms have been proposed to explain the unique thermoelectric performance of Yb-filled $CoSb_3$. One proposed mechanism is the linear dispersion (Kane-type) of the valence band in $CoSb_3$ [29–35]. In $CoSb_3$, there is one quasilinear nonparabolic valence band, one quasilinear conduction band, and one triply degenerated parabolic conduction band at Γ point [31]. However, a theoretical study suggests that the nonparabolic band dispersions do not increase S and are not beneficial to thermoelectric performance [3]. This study suggests that a secondary conduction band near the conduction band minimum in $CoSb_3$ could be used to explain the high performance of Yb-filled $CoSb_3$, and these two bands converge at high temperatures. Another proposed mechanism is that several new band minima due to Yb filling should make a substantial contribution to the electrical transport, contrary to the band convergence picture of the

---

*xjchen2@gmail.com

secondary conduction band with the primary band in $CoSb_3$ [36]. The reason for the significant increase in σ while slightly affected S remains unsettled. These conflicts call for a unique mechanism responsible for the electrical transport properties of filled skutterudites.

$CoSb_3$ has been predicted to be very near a critical point of topological transition from first-principles calculations [37,38]. This means that there are underlying topological states in $CoSb_3$, but the evidence for surface states, topological invariants, and experiments is lacking. The topological transition in $CoSb_3$ can be induced by applying an appropriate strain [37–40]. Filling atoms into the voids of $CoSb_3$ can expand the lattice constant and change the internal parameters, and hence may have the same effect with strain. In addition, for thermoelectric applications, our attention is focused on the filled skutterudite due to its relatively high conversion efficiency. A recent study has pointed out that two filled skutterudites, $CeOs_4As_{12}$ and $CeOs_4Sb_{12}$, are topological insulators through *ab initio* calculations [41]. However, up to now, little information about the topological properties of the most efficient Yb-filled $CoSb_3$ skutterudites has been available, either theoretically or experimentally. Two important questions have not been settled. One is regarding whether topological states exist in Yb-filled $CoSb_3$ or not. The other is about how the topological states affect the thermoelectric properties if they indeed exist.
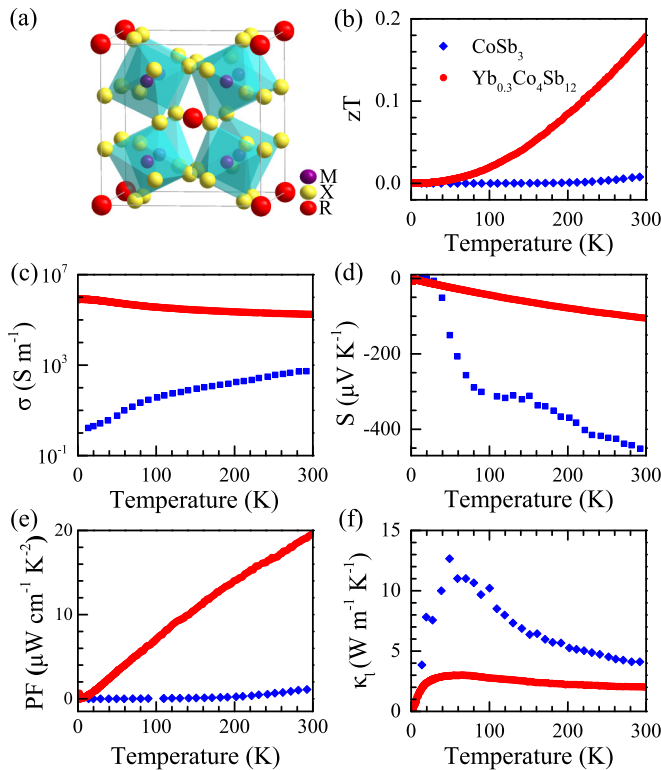
Taking a highly efficient Yb-filled $CoSb_3$ skutterudite as an example in this paper, we explore its possible topological properties through the combination of first-principles calculations and low-temperature electrical transport measurements. The topological states are identified based on the presence of the surface state. The influence of the topological states on the electrical transport properties of Yb-filled $CoSb_3$ skutterudite is investigated from a combination of theoretical analysis and experimental results.

II. Method

A. Experimental details

The sample was prepared by a melt spinning and spark plasma sintering process detailed elsewhere [42]. An energy dispersive spectrometer (EDS, OXFORD) was employed to confirm the actual composition of the sample. A RigakuD/MAX-2550PC diffractometer was used to determine the sample structure under Cu-Kα radiation with a wavelength of 1.5406 Å.

The thermoelectric properties were characterized utilizing the thermal transport option of a physical property measurement system from Quantum Design at temperatures 2–300 K. The Hall effect measurements were performed by employing the resistivity option in the magnetic field at temperatures ranging from 2 to 300 K. The resistivity (ρ) was measured by using the standard four-probe method. To eliminate the transverse (longitudinal) ρ component from the misalignment of contacts, we obtained the ρ_{xx} and ρ_{xy} through $\rho_{xx} = (\rho_{xx}(+H) + \rho_{xx}(-H))/2$ and $\rho_{xy} = (\rho_{xx}(+H) - \rho_{xx}(-H))/2$, respectively.

B. Theoretical calculations

The electronic structure calculations were performed based on density functional theory (DFT) employed in the Vienna *Ab initio* Simulation Package [43]. The electronic properties were calculated by the projector augmented wave method [43,44] with a Perdew-Burke-Ernzerbof-type generalized gradient approximation [45]. All the lattice parameters and atomic positions were fully relaxed in the unit cell. The plane-wave basis was set with a cutoff energy of 520 eV. Spin-orbit coupling was included in our calculations. The maximally localized Wannier functions were constructed by employing the WANNIER90 package [46]. The open-source software package (WANNIERTOOLS) [47] was used to investigate the topological nature of the projected (001) surface.

III. RESULTS AND DISCUSSION

A. Characterization of thermoelectric parameters

Figure 1(a) illustrates the crystal structure of filled skutterudites. Skutterudite compounds have the general formula of MX_3 (M is Co, Rh, or Ir; X is P, As, or Sb) [48]. These compounds are body-centered cubic with space group $Im\bar{3}$ and space group No. 204. The skutterudite crystal structure consists of eight corner-sharing octahedra. The center of these octahedra is the M atom and the corners are the X atoms. The octahedra are tilted so the X atoms form rectangular X_4 rings. The linked octahedra generates a void in the center of

FIG. 1. Crystal structure and temperature-dependent thermoelectric properties of $Yb_{0.3}Co_4Sb_{12}$. (a) Crystal structure of the filled-skutterudite. (b) Figure of merit zT. (c) Electrical conductivity σ. (d) Seebeck coefficient S. (e) Power factor PF. (f) Lattice thermal conductivity κ_l. The data points of $CoSb_3$ are taken from Ref. [51] for the comparison.

the lattice. Filling this void with a guest atom, such as rare earth, can form the so-called filled-skutterudite structure [49] with the general formula RM_4X_{12}, as shown in Fig. 1(a). The filling atoms can increase the lattice constant and change the structural parameters. The lattice constant has been reported to increase with the amount of filling for Tl-filled [50], Yb-filled [19,51], Ba-filled [52], and triple-element-filled skutterudites [23]. The most significant change is the bond length for the short Sb-Sb bond, which becomes closer to a square in the filled skutterudites (Yb, Ce, Ba)Co_4Sb_{12} [53]. Figures 1(b)–1(f) show the electrical and thermal transport properties of $Yb_{0.3}Co_4Sb_{12}$ from 2 to 300 K, compared with those of pristine $CoSb_3$ [51]. As shown in Fig. 1(b), zT of $Yb_{0.3}Co_4Sb_{12}$ increases with increasing temperature and reaches 0.18 at room temperature, significantly larger than that of $CoSb_3$. This enhancement on zT is in agreement with previous studies [23,54].

The temperature-dependent κ_l is presented in Fig. 1(f). The κ_l was obtained from the total κ by subtracting κ_e. The κ_e was calculated from the Wiedemann-Franz law $\kappa_e = L\sigma T$, where L is the Lorenz factor and its typical values are 2.45×10^{-8} and 1.49×10^{-8} V^2K^{-2} for metals and intrinsic semiconductors, respectively [1]. The κ_l varies with temperature in a typical λ shape. It increases rapidly with increasing temperature and reaches a maximum (approximately 3.0 $WK^{-1}m^{-1}$) around 66 K, then declines gradually. Compared with $CoSb_3$, the κ_l of $Yb_{0.3}Co_4Sb_{12}$ is significantly reduced. The value of κ_l in $Yb_{0.3}Co_4Sb_{12}$ is 2 $WK^{-1}m^{-1}$ at room temperature, lower than that of other single-filled skutterudites and comparable to that of the multifilled skutterudites [23]. The mechanism behind the low κ_l has been extensively studied, including strong anharmonicity, the hybridization of the guest atom and host lattice, the flat guest mode avoided crossing with the acoustic-phonon mode, and the significant contribution of optical phonons [15,16,24–28]. Therefore, the reason for the low κ_l is not discussed in detail here.

Although κ_l is largely reduced, the electrical properties of $Yb_{0.3}Co_4Sb_{12}$ only slightly deteriorate. As shown in Fig. 1(c), σ of $Yb_{0.3}Co_4Sb_{12}$ increases with decreasing temperature and then saturates at low temperatures, exhibiting a heavily doped semiconductor behavior. However, $CoSb_3$ shows semiconducting behavior down to 10 K. Notably, the value of σ in $Yb_{0.3}Co_4Sb_{12}$ is higher than that of $CoSb_3$ by several orders of magnitude. The temperature dependence of S is demonstrated in Fig. 1(d). The negative value of S decreases nearly linearly with increasing temperature, consistent with an n-type degenerate semiconductor character. Compared with $CoSb_3$, the absolute value of S in $Yb_{0.3}Co_4Sb_{12}$ is slightly lower, reduced from 450 μVK^{-1} in $CoSb_3$ to 105 μVK^{-1} in $Yb_{0.3}Co_4Sb_{12}$ at room temperature. Similar trends in σ and S of $Yb_{0.3}Co_4Sb_{12}$ can be found in other filled skutterudites [23,35].

By combining σ and S, we can obtain the temperature dependence of PF for $Yb_{0.3}Co_4Sb_{12}$. The results are demonstrated in Fig. 1(e). As can be seen, PF increases with increasing temperature and reaches 20 $\mu Wcm^{-1}K^{-2}$ at room temperature. This PF value is comparable to those in other filled skutterudites [23] and is several orders of magnitude higher than that in $CoSb_3$. The substantial improvement of PF is predominantly due to the dramatically increased σ with a subtle decrease in S.
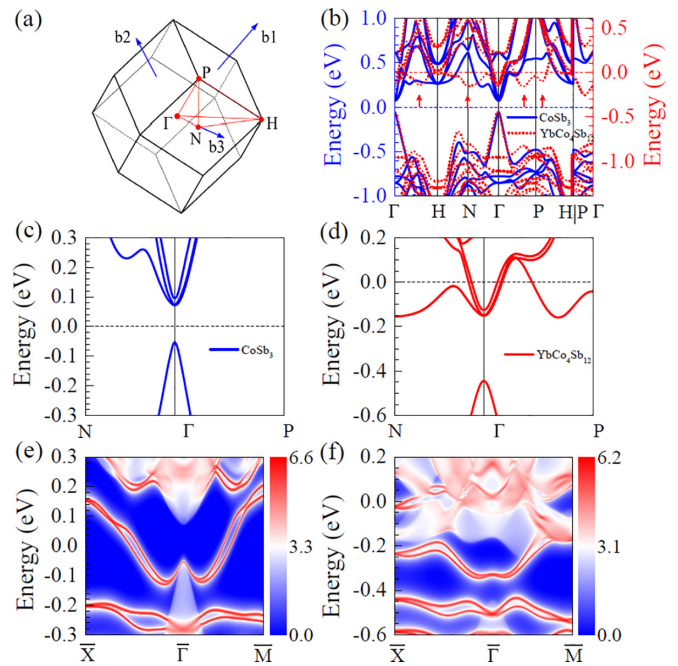

FIG. 2. (a) The first Brillouin zone. (b) The bulk electronic band structure of $CoSb_3$ and $YbCo_4Sb_{12}$. The energy reference is set to the Fermi level. Additional conduction band minima in $YbCo_4Sb_{12}$ are noted by the vertical arrows. The zoom of the bulk structure of $CoSb_3$ (c) and $YbCo_4Sb_{12}$ (d), respectively. Energy and momentum dispersion with the local density of states on the (001) surface of $CoSb_3$ (e) and $YbCo_4Sb_{12}$ (f), respectively.

The increase in σ and the decrease in the absolute value of S are related to the increase in n [35] of $Yb_{0.3}Co_4Sb_{12}$. Filling the voids with Yb atoms provides additional electrons to the skutterudite, resulting in an increase in n. Generally, σ is proportional to n and S is inversely related to n. However, the values of n in filled skutterudites and $CoSb_3$ are quite different ($10^{20} \sim 10^{21}$ cm^{-3} for the filled versus $10^{17} \sim 10^{18}$ cm^{-3} for $CoSb_3$) [55]. Therefore, assessing the extent to which the filled atoms affect electrical properties is difficult. The high σ is also attributed to the high μ resulting from the linear bands [29,30,32–34]. The linear bands correspond to a small single-band effective mass (m_b^*), which is not conducive to S. Whereas, unlike the significant increase in σ, S only exhibits a moderate decline. The multiband effect can affect S in $CoSb_3$. This picture is not applicable for filled skutterudites [3,36]. All clues point to the importance of the particular band structure in Yb-filled $CoSb_3$.

B. Topological states from calculations

Figure 2(a) depicts the Brillouin zone of body-centered cubic, Γ, H, N, and P are high-symmetry points. The band structures of $CoSb_3$ and $YbCo_4Sb_{12}$ are plotted in Fig. 2(b). Consistent with previous studies [3,29,31], our calculations reveal that $CoSb_3$ is a direct band-gap semiconductor with one valence band and three degenerated conduction bands at the Γ point. The valence bands are mainly occupied by the orbital electrons of Co-p/d and Sb-p, while the conduction bands are composed of orbital electrons of Co-d. Unlike
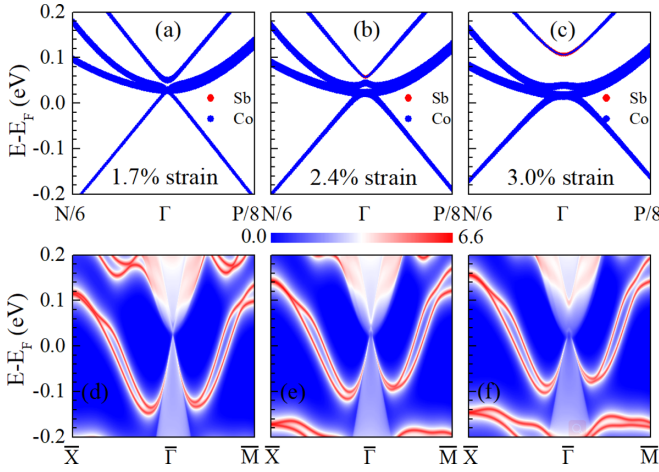
FIG. 3. (a)–(c) Band structures of CoSb$_3$ near k=0, showing the band crossing as the valence band rises due to the strain. (a) Before transition, strain = 1.7%. (b) At the critical point, strain = 2.4%. (c) After the transition, strain = 3.0%. (d)–(f) The corresponding energy and momentum dispersion with the local density of states on the (001) surface.

the usual parabolic bands, the valence and conduction bands near the Fermi surface show linear dispersion at Γ. This result agrees with previous electronic structure calculations on CoSb$_3$ [29,31].

The band-gap values obtained from the DFT calculations for CoSb$_3$ and YbCo$_4$Sb$_{12}$ are 0.12 eV and 0.29 eV, respectively. These values are comparable to those previously reported from other calculations [31,35]. The effective mass can be obtained by fitting the bands close to the Fermi level via the Kane model [31]. The effective mass of the valence band for CoSb$_3$ is $m^*/m_0 = 0.068, 0.067$, and 0.077 for the $\Gamma \rightarrow$ H, $\Gamma \rightarrow$ N, and $\Gamma \rightarrow$ P directions. The effective mass of the conduction band is $m_e/m_0 = 0.31$. Our calculated effective masses agree well with previous studies [31]. Correspondingly, the effective mass for YbCo$_4$Sb$_{12}$ is $m^*/m_0 = 0.091$, 0.089, and 0.095, $m_e/m_0 = 0.41$. The increase in the effective masses of YbCo$_4$Sb$_{12}$ is also consistent with previous studies [35].

Compared with the parent compound, the electronic band structure of Yb-filled CoSb$_3$ does not change significantly, in accord with previous calculations [3,29,36]. The main differences lie in the following three aspects. First, Yb filling into CoSb$_3$ leads to an increase in the band gap, agreeing with previous studies [36]. Similar behavior has been found in previous studies on CaCo$_4$Sb$_{12}$ and SrCo$_4$Sb$_{12}$ [56], thereby suggesting that this effect is independent of the sort of the filling atom [36]. Second, compared with CoSb$_3$, the quasilinear conduction band and the parabolic conduction band triply degenerated at Γ have little variation and are slightly flattened, as shown in Figs. 2(c) and 2(d). These results are consistent with the increase in the effective masses of YbCo$_4$Sb$_{12}$ with respect to CoSb$_3$, which may be due to the linear conduction band or a change in the band structure with increasing n [35]. Third, the additional conduction band minima appear near the bottom of the conduction band at Γ for YbCo$_4$Sb$_{12}$. The new

band minima are marked in Fig. 2(b). Especially, there exists a relatively flat band at N.

According to Kane dispersion [57], the increased band gap in YbCo$_4$Sb$_{12}$ improves the density-of-states effective mass (m^*) and thus S. A similar phenomenon has been reported in efficient thermoelectric materials [2]. In addition, the additional conduction band minima in YbCo$_4$Sb$_{12}$ increase the valley degeneracy (N_V). Generally, N_V contributes to m^* through $m^*=N_V^{2/3}m_b^*$ [58], where m_b^* is the single-band effective mass. The increase of N_V enhances m^* without affecting μ [2], which is beneficial to PF and thus zT. In CoSb$_3$, the secondary conduction band between N and Γ has a high N_V with 12 isolated pockets [3,59]. This high N_V is comparable to that in PbTe, another high-efficient thermoelectric material with $zT \sim 2$ [2]. There are more additional conduction band minima in YbCo$_4$Sb$_{12}$ than those in CoSb$_3$. This result has been confirmed by previous theoretical study [36]. Because of this, we can reasonably infer that N_V in YbCo$_4$Sb$_{12}$ is higher than that in CoSb$_3$. The high N_V in Yb-filled CoSb$_3$ has also been indicated from the increase in m^* [36]. Nevertheless, compared with CoSb$_3$, Yb-filled skutterudite has a relatively small S from the experiment, as shown in Fig. 1(d).

Previous studies have shown that low m_b^* leads to high thermoelectric performance [60]. This is because μ is proportional to $m_b^{*-5/2}$ for most high-performance thermoelectric materials [2]. High μ is achieved in materials with light m_b^*. Additionally, the optimal PF is related to $\mu m^{*3/2}$ and m_I^{*-1} [2,58,61]. The m_I^* parameter is the inertial effective mass. For an isotropic band, m_I^* is equal to m_b^*. Although lowering m_b^* results in a small S, PF increases. Consequently, the linear valence band with low m_b^* in CoSb$_3$ explains the high μ observed in lightly doped p-type CoSb$_3$ and is beneficial to zT [30]. Compared with the other triply degenerated parabolic conduction bands, the linear conduction band in YbCo$_4$Sb$_{12}$ has relatively low m_b^* and should have the same effect. This behavior agrees with previous studies for CoSb$_3$ and filled skutterudites [29,32–34].

The linear dispersions from the valence and conduction bands produce unique consequences which are related to the topological insulator transition [29,37,38,57]. CoSb$_3$ has been predicted to be near the strain-induced transition to a topological-insulator phase through a topological quantum critical point by bulk band structure calculations [37]. However, the topological surface states and $\mathbb{Z}2$ topological index are still lacking. For this purpose, we show the surface states of CoSb$_3$ and YbCo$_4$Sb$_{12}$ in Figs. 2(e) and 2(f), respectively. The (001) surface is selected to explore the surface states. Metallic surface states at the (001) surface in CoSb$_3$ and YbCo$_4$Sb$_{12}$ are observed. The $\mathbb{Z}2$ topological index is a parity criteria to determine the topological features [62]. To determine their topological properties, we calculated the $\mathbb{Z}2$ indexes of CoSb$_3$ and YbCo$_4$Sb$_{12}$. CoSb$_3$ is found to be topologically trivial with $\mathbb{Z}2$ (0;000), while YbCo$_4$Sb$_{12}$ is found to be topologically nontrivial with $\mathbb{Z}2$ (1;111). This theoretical result supports the existence of the topological surface states in YbCo$_4$Sb$_{12}$.

To prove the reliability of the calculation results, we calculated the bulk electronic structure and surface states of CoSb$_3$ under tensile strain, as shown in Fig. 3. To obtain the topological transition, we applied 1.7%, 2.4%, and 3.0% strain
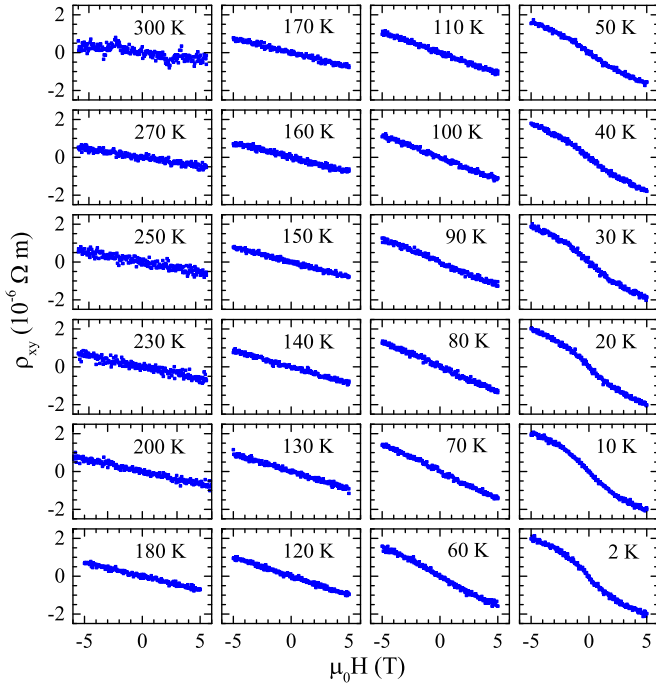
FIG. 4. Hall resistivity (ρ_{xy}) of Yb$_{0.3}$Co$_4$Sb$_{12}$ in the applied magnetic fields at various temperatures.

FIG. 5. (a)–(c) Magnetic-field-dependent Hall conductivity (σ_{xy}) of Yb$_{0.3}$Co$_4$Sb$_{12}$ at temperatures of 2, 10, and 20 K. The blue circles denote the raw data points, with the solid red lines denoting the whole fitting results. The black line represents the relevant surface term. (d)–(f) The corresponding magnetoresistance (MR) ($\rho_H/\rho_0 - 1$) of Yb$_{0.3}$Co$_4$Sb$_{12}$ at temperature of 2, 10, and 20 K.

on CoSb$_3$. The bulk electronic structures are demonstrated in Figs. 3(a)–3(c), respectively. The corresponding surface states are shown in Figs. 3(d)–3(f), respectively. When the strain is 1.7%, the $\mathbb{Z}2$ index is (0;000), which means that the surface state is topologically trivial. When the strain is 2.4% and 3.0%, the band inversion occurs between the orbital electrons of Co-d and Sb-p. The corresponding $\mathbb{Z}2$ indexes are both (1;000), supporting the nontrivial topological surface states in CoSb$_3$. This result agrees with previous predictions [37,38]. Furthermore, the strain in CoSb$_3$ can be induced by filling the voids such as Yb atoms, resulting in the expansion of the lattice constant and the change of the bond length for the short Sb-Sb bond. Therefore, filling the voids with atoms provides an additional approach to realizing topological insulators.

C. Experimental evidence for the topological state

To seek the experimental evidence of topological states, we also performed Hall effect measurements. Figure 4 demonstrates the magnetic field dependence of the Hall resistivity (ρ_{xy}) for Yb$_{0.3}$Co$_4$Sb$_{12}$ at temperatures below 300 K. Since ρ_{xy} is always negative from 0 to 5 T, the dominant carriers are electrons. With decreasing temperature, the nonlinear behavior becomes pronounced. This nonlinear behavior indicates the existence of multiple carriers with different concentrations and mobilities.

Figure 5 shows the Hall conductivity (σ_{xy}) and the longitudinal magnetoresistance (MR) at temperature of 2, 10, and 20 K. σ_{xy} is calculated from $\sigma_{xy} = \rho_{xy}/(\rho_{xx}^2 + \rho_{xy}^2)$. MR is defined by MR $= (\rho_{xx}(H)/\rho_{xx}(0) - 1) \times 100\%$, where $\rho_{xx}(0)$ and $\rho_{xx}(H)$ are the longitudinal resistivity measured at zero and applied magnetic field, respectively. In agreement with ρ_{xy}, σ_{xy} exhibits distinct nonlinear behavior. MR is
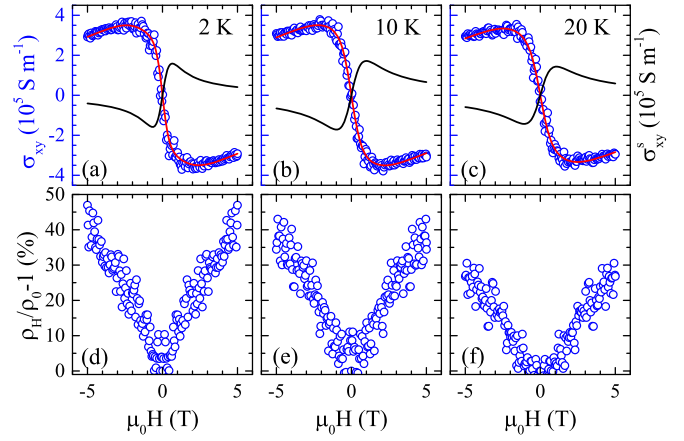
approximately linear in the applied magnetic field, in contrast with the quadratic response to MR seen in ordinary semiconductors.

The resonance σ_{xy} and linear MR are two important characters of nontrivial topological states [10,63]. In topological insulators, the superposition of the surface and the bulk transport channels results in the nonlinear σ_{xy} [10]. Therefore, the nonlinear σ_{xy} observed in Yb$_{0.3}$Co$_4$Sb$_{12}$ can be considered to be a result of the topological states. The linear MR is attributed to the topological surface states and associated with the linear bands [64–66], matching well with quantum linear MR theory. According to previous studies, the linear MR in Yb$_{0.3}$Co$_4$Sb$_{12}$ may result from the weak antilocalization of the topological surface states and the weak localization of the bulk [67,68]. Similar behavior has been observed in topological insulators Bi$_2$Te$_3$ and Bi$_2$Se$_3$ [10,69]. As a result, the anomalous σ_{xy} and MR provide experimental evidence in favor of the nontrivial topological states in Yb$_{0.3}$Co$_4$Sb$_{12}$.

To examine the contributions of the topological surface states to the electrical transport properties, we fitted σ_{xy} with the following formulas [10]:

$$\sigma_{xy} = \sigma_{xy}^b + \sigma_{xy}^s, \tag{1}$$

$$\sigma_{xy}^b = n_{\text{eff}} e \mu_b \frac{\mu_b B}{1 + (\mu_b B)^2}, \tag{2}$$

$$\sigma_{xy}^s = \frac{2\pi^3}{h^2 t} \frac{B\ell^2}{1 + (\mu_s B)^2}, \tag{3}$$

where σ_{xy}^b is the bulk Hall conductivity, σ_{xy}^s is the surface Hall conductivity (in cm^{-3}), t is the crystal thickness, n_{eff} is the effective bulk carrier concentration, μ_b is the bulk carrier mobility, μ_s is the surface carrier mobility, ℓ is the surface mean free length, and B is the magnetic flux density, respectively. Important transport parameters can be obtained from the fitting to the obtained Hall conductivities, as summarized in Table I. Notably, μ_s is comparable to that of Bi$_2$Te$_3$ [10] and about five times larger than the bulk value. The relatively

TABLE I. Summary of the bulk mobility μ_b (in cm^{2}V^{-1}s^{-1}), bulk effective carrier concentration n_{eff} (in cm^{-3}), surface mobility μ_s (in cm^{2}V^{-1}s^{-1}), and surface mean free length ℓ (in nm) of Yb$_{0.3}$Co$_4$Sb$_{12}$ at low temperatures, in comparison with the results of Bi$_2$Te$_3$ at 0.3 K [10].

	Yb$_{0.3}$Co$_4$Sb$_{12}$			Bi$_2$Te$_3$
T (K)	2	10	20	0.3
μ_b	3184.7	2983.5	2909.6	860
n_{eff}	1.1×10^{19}	1.0×10^{19}	1.0×10^{19}	6.9×10^{15}
μ_s	15209.2	10033.4	9289.3	9000
ℓ	90.5	76.5	67.2	235

large μ_s value is due to the topological surface states with linear energy dispersion. It is favorable for high σ. The significantly enhanced σ of Yb$_{0.3}$Co$_4$Sb$_{12}$ thus benefits from the topological surface states.

D. Other electrical transport properties

Considering the contribution of the topological states, we fit σ_{xy} at different temperatures and obtain the temperature dependence of both n_{eff} and μ_b. The n_{eff} value of Yb$_{0.3}$Co$_4$Sb$_{12}$ has a nearly optimal absolute value of 10^{19} cm^{-3} as shown in Fig. 6(a), which is about two orders of magnitude higher than the parent compound [55]. With decreasing temperature, n_{eff} exhibits a gradual decrease behavior. At low temperatures, it has a gentle increase. On the contrary, μ_b increases dramatically from 123 to 3185 cm^{2}V^{-1}s^{-1} with decreasing temperature, as shown in Fig. 6(b). The temperature-dependent μ follows a $T^{-3/2}$ behavior, implying that acoustical phonon scattering dominates the scattering mechanism [70]. In this case, μ is proportional to $1/m_b^{*5/2}$ [58]. The temperature-dependent μ in reality has the quantum origin of the linear MR in Yb$_{0.3}$Co$_4$Sb$_{12}$. High μ is an important signature for topological insulators.

Figure 7(a) shows the temperature-dependent m_S^*. For thermoelectric materials, m_S^* refers to m^*. m_S^* is given by using the S and n determined from the Hall effect [71]:

$$
\frac{m_S^*}{m_e} = 0.924 \left(\frac{300\text{K}}{T} \right) \left(\frac{n}{10^{20}\text{cm}^{-3}} \right)^{2/3}
$$

$$
\times \left[\frac{3\left(\exp\left[\frac{|S|}{k_B/e}\right] - 0.17\right)^{2/3}}{1 + \exp\left[-5\left(\frac{|S|}{k_B/e} - \frac{k_B/e}{|S|}\right)\right]} \right.
$$

$$
\left. + \frac{\frac{|S|}{k_B/e}}{1 + \exp\left[5\left(\frac{|S|}{k_B/e} - \frac{k_B/e}{|S|}\right)\right]} \right]. \tag{4}
$$

This equation can give an estimation of m_S^*. For the absolute value of S larger than 20 μVK^{-1}, the uncertainty of the result is about 3%. Although the abrupt change of m_S^* at 2 K is not precise, the changing trend of m_S^* can be well captured.

As shown in Fig. 7(a), m_S^* increases monotonically with increasing temperature, opposed to the μ_b behavior. Figure 7(b) shows m_S^* as a function of n of Yb$_{0.3}$Co$_4$Sb$_{12}$. m_S^* increases with an increase in n, following an $n^{1/2}$ dependence. Because
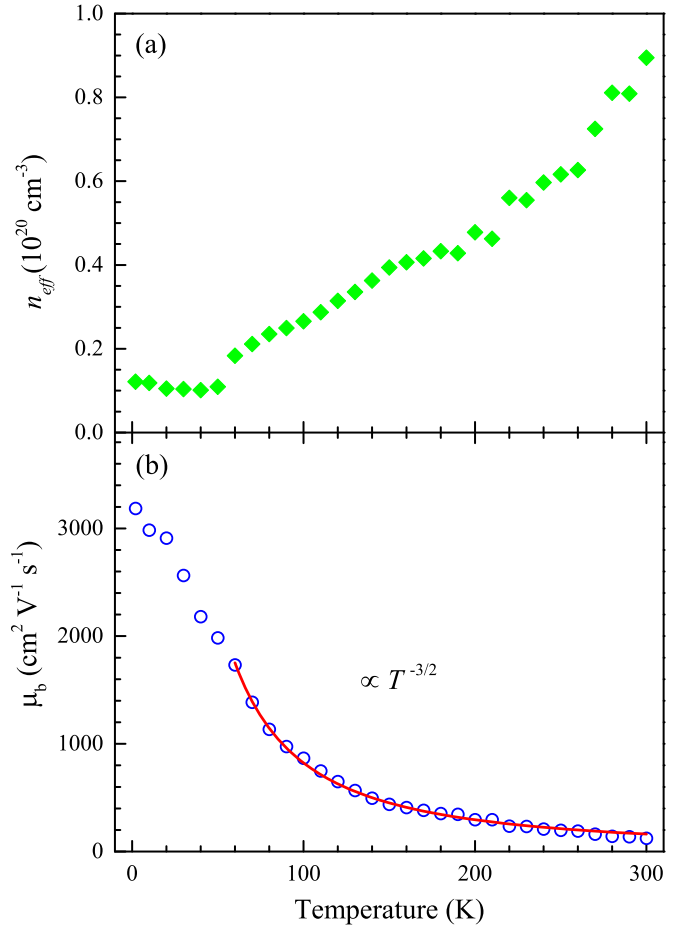

FIG. 6. Temperature dependence of (a) the effective carrier concentration (n_{eff}) and (b) the bulk carrier mobility (μ_b) of Yb$_{0.3}$Co$_4$Sb$_{12}$.

the m_S^* value changes with n, the bands are not parabolic [72]. This behavior of m_S^* for Yb$_{0.3}$Co$_4$Sb$_{12}$ can be attributed to the linear bands associated with the topological surface states.

The effect of the nonparabolic properties on m_S^* can be summarized in a two-band Kane model [30,32–34]:

$$
m^* = m_e \left(1 + \frac{2\eta}{\Delta E} \right), \tag{5}
$$

where m_e is the effective mass at the bottom of the band, η is the reduced Fermi energy, and $\Delta E = E_g / k_B T$ is the reduced energy gap. In the nonparabolic band model, m_S^* in CoSb$_3$ would follow $n^{1/3}$ [29]. The quasilinear dispersion band model agrees well with experimental results of some filled skutterudites R_xCo$_4$Sb$_{12}$ (R=Nd, Tl, Ba, La, Ce, Yb) [3,29,35,39,40]. At low temperatures, the bands in these materials become linear rather than parabolic, leading to the m_S^* reduction. In addition, a previous study has shown that m_S^* of CoSb$_3$ decreases in the quasilinear dispersion band relative to that in a parabolic band [3]. Therefore, a previous study has attributed the increase of m_S^* with n to the multiple conduction bands rather than the linear bands [3]. In our present study, we find that m_S^* in Yb-filled CoSb$_3$ varies with n by
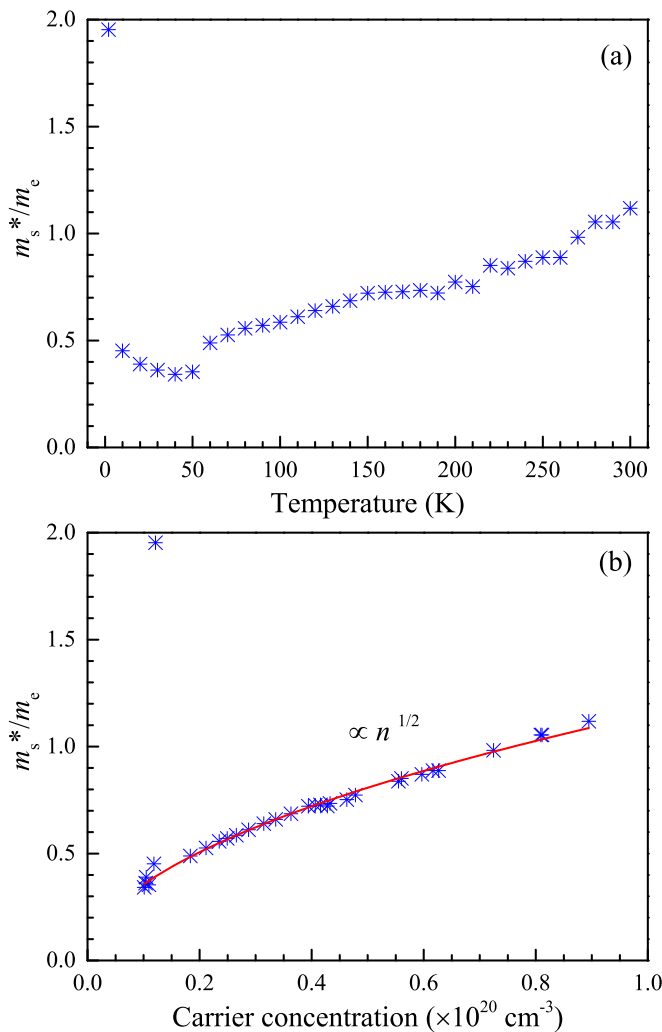
FIG. 7. (a) Temperature dependence of the Seebeck effective mass (m_S^*) in $Yb_{0.3}Co_4Sb_{12}$. (b) Carrier concentration dependence of the Seebeck effective mass (m_S^*).

1/2 instead of 1/3 observed in the parent compound. In contrast to the parent $CoSb_3$, Yb-filled $CoSb_3$ possesses both the topological surface states as well as new additional conduction band minima. As a result, the dependence of m_S^* on n in Yb-filled $CoSb_3$ deviates slightly from that in the parent. Therefore, the n dependence of m_S^* in Yb-filled $CoSb_3$ is a combined result of both the linear band and multiple conduction bands associated with the topological states.

E. Topological state effect

Previous studies have predicted that applying the strain on $CoSb_3$ could induce topological insulators [37,38]. Nonetheless, the prominent features of topological insulators, such as the surface states and the $\mathbb{Z}2$ invariants, as well as experimental evidence, remain lacking. Our results fill in this gap. In our calculations, a topological transition is obtained by applying a 2.4% strain on $CoSb_3$. The corresponding surface states are found to be topologically nontrivial with $\mathbb{Z}2$ (1;000). Likewise, filling the voids in the parent with atoms can have the same effect with strain, providing an additional

way to gain topological states. Subsequently, the surface states with $\mathbb{Z}2$ (1;111) in Yb-filled $CoSb_3$ are attained, supporting the nontrivial topological states. It is worth noting that the transport evidence for topological states in Yb-filled $CoSb_3$ is recognized from anomalous σ_{xy} and MR.

The existence of topological states makes it possible to optimize PF without losing σ or S as a sacrifice. The topological states result from the nonparabolic (Kane) bands with small m_b^*. Small m_b^* favors μ because of the inverse relationship between these two parameters. The linear bands associated with topological states thus enhance σ and PF due to the extremely high μ. Meanwhile, the obtained n and m_S^* from the experimental measurements, in turn, verify the linear bands. A previous study has found that the electrical transport properties of $CoSb_3$ are determined by the linear dispersion when n is not less than $n_c = 3 \times 10^{16}$ cm^{-3} [29]. For filled skutterudites, the n values are all much higher than n_c. Accordingly, the electrical transport properties of Yb-filled $CoSb_3$ are dominated by the linear dispersion of the bands related to the topological states. The $n^{1/2}$ dependence of m^* in Yb-filled $CoSb_3$ implies the contribution of the linear bands related to the topological states.

In addition, the additional band minima in the nontrivial topological Yb-filled $CoSb_3$ furthermore contribute to PF. A previous study has attributed the increase in S to the high N_V of the secondary band in $CoSb_3$ [3]. On the contrary, we find that the secondary band in $CoSb_3$ does not contribute to the S increase in Yb-filled $CoSb_3$. However, the S enhancement results from the new conduction band minima. According to our calculations, Yb-filled $CoSb_3$ has more additional conduction band minima than $CoSb_3$, providing relatively high N_V. The high N_V benefits m_S^* and thus favors S. Consequently, S does not show a dramatic decrease. Based on the greatly enhanced σ and slightly reduced S, PF in $Yb_{0.3}Co_4Sb_{12}$ should be improved comprehensively.

The typical method to improve the performance of thermoelectric materials is through the band-structure engineering. This approach can generate band convergence or resonate states by doping atoms into the parent compounds [2–5]. Consequently, S can be enhanced by increasing m^*. However, a high m^* is detrimental to μ, and thus σ. Therefore, to balance S and σ for the optimized PF, it is necessary to exactly manage the doping ratio. Topological states in filled skutterudites can enhance σ while keeping S scarcely affected. Hence, introducing topological states into thermoelectric materials is a simple and efficient approach to boosting PF. Due to the demand of high-efficiency thermoelectric materials for the technological applications, introducing the nontrivial topological states may guide the discovery of high-performance thermoelectric materials.

IV. CONCLUSIONS

We have ascertained the topological states in Yb-filled $CoSb_3$ skutterudite from the combined first-principles calculations and electrical transport measurements. The existence of the topological states is evidenced by the resonance Hall conductivity and linear MR at low temperatures. The effect of topological states on the thermoelectric performance is further examined. The results reveal that the topological states

originating from the linear bands lead to the low single-band effective mass and the high carrier mobility, thus yielding the large PF. The new band minima are found to contribute to the Seebeck coefficient due to the increase in both the valley degeneracy and the density-of-states effective mass. A unqiue mechanism is thus proposed to account for the widely observed increase of the PF in filled skutterudites. Our synergistic theoretical and experimental efforts shed insight on the correlation between the topological states and the thermoelectric performance, which might be beneficial in designing highly efficient thermoelectric materials for better heat energy harvesting.

[1] G. J. Snyder and E. S. Toberer, Complex thermoelectric materials, Nat. Mater. **7**, 105 (2008).

[2] Y. Z. Pei, X. Y. Shi, A. LaLonde, H. Wang, L. D. Chen, and G. J. Snyder, Convergence of electronic bands for high performance bulk thermoelectrics, Nature (London) **473**, 66 (2011).

[3] Y. L. Tang, Z. M. Gibbs, L. A. Agapito, G. D. Li, H. S. Kim, M. B. Nardelli, S. Curtarolo, and G. J. Snyder, Convergence of multi-valley bands as the electronic origin of high thermoelectric performance in $CoSb_3$ skutterudites, Nat. Mater. **14**, 1223 (2015).

[4] J. P. Heremans, V. Jovovic, E. S. Toberer, A. Saramat, K. Kurosaki, A. Charoenphakdee, S. Yamanaka, G. J. Snyder, Enhancement of thermoelectric efficiency in PbTe by distortion of the electronic density of states, Science **321**, 554 (2008).

[5] Q. Y. Zhang, H. Wang, W. S. Liu, H. Z. Wang, B. Yu, Q. Zhang, Z. T. Tian, G. Ni, S. Lee, K. Esfarjani, G. Chen, and Z. F. Ren, Enhancement of thermoelectric figure-of-merit by resonant states of aluminium doping in lead selenide, Energy Environ. Sci. **5**, 5246 (2012).

[6] H. J. Zhang, C. X. Liu, X. L. Qi, X. Dai, Z. Fang, and S. C. Zhang, Topological insulators in Bi_2Se_3, Bi_2Te_3 and Sb_2Te_3 with a single Dirac cone on the surface, Nat. Phys. **5**, 438 (2009).

[7] L. Müchler, F. Casper, B. H. Yan, S. Chadov, and C. Felser, Topological insulators and thermoelectric materials, Phys. Status Solidi RRL **7**, 91 (2013).

[8] Y. L. Chen, J. G. Analytis, J. H. Chu, Z. K. Liu, S. K. Mo, X. L. Qi, H. J. Zhang, D. H. Lu, X. Dai, Z. Fang, S. C. Zhang, I. R. Fisher, Z. Hussain, and Z. X. Shen, Experimental realization of a three-dimensional topological insulator, Bi_2Te_3, Science **325**, 178 (2009).

[9] Y. Xia, D. Qian, D. Hsieh, L. Wray, A. Pal, H. Lin, A. Bansil, D. Grauer, Y. S. Hor, R. J. Cava, and M. Z. Hasan, Observation of a large-gap topological-insulator class with a single Dirac cone on the surface, Nat. Phys. **5**, 398 (2009).

[10] D. X. Qu, Y. S. Hor, J. Xiong, R. J. Cava, and N. P. Ong, Quantum oscillations and Hall anomaly of surface states in the topological insulator Bi_2Te_3, Science **329**, 821 (2010).

[11] C. Y. Chen, S. L. He, H. M. Weng, W. T. Zhang, L. Zhao, H. Y. Liu, X. W. Jia, D. X. Mou, S. Y. Liu, J. F. He, Y. Y. Peng, Y. Feng, Z. J. Xie, G. D. Liu, X. L. Dong, J. Zhang, X. Y. Wang, Q. J. Peng, Z. M. Wang, S. J. Zhang *et al.*, Robustness of topological order and formation of quantum well states in topological insulators exposed to ambient environment, Proc. Natl. Acad. Sci. USA **109**, 3694 (2012).

[12] Y. Xiao, D. Y. Wang, B. C. Qin, J. F. Wang, G. T. Wang, and L. D. Zhao, Approaching Topological Insulating States Leads to high thermoelectric performance in *n*-type PbTe, J. Am. Chem. Soc. **140**, 13097 (2018).

[13] L. C. Chen, P. Q. Chen, W. J. Li, Q. Zhang, V. V. Struzhkin, A. F. Goncharov, Z. F. Ren, and X. J. Chen, Enhancement of thermoelectric performance across the topological phase transition in dense lead selenide, Nat. Mater. **18**, 1321 (2019).

[14] N. T. Hung, J. M. Adhidewata, A. R. T. Nugraha, and R. Saito, Enhanced thermoelectric performance by van Hove singularities in the density of states of type-II nodal-line semimetals, Phys. Rev. B **105**, 115142 (2022).

[15] G. A. Slack, in *CRC Handbook of Thermoelectrics*, edited by D. M. Rowe (CRC, Boca Raton, FL, 1995).

[16] G. S. Nolas, D. T. Morelli, and T. M. Tritt, Skutterudites: A phonon-glass-electron-crystal approach to advanced thermoelectric energy conversion applications, Annu. Rev. Mater. Sci. **29**, 89 (1999).

[17] X. Shi, H. Kong, C.-P. Li, C. Uher, J. Yang, J. R. Salvador, H. Wang, L. Chen, and W. Zhang, Low thermal conductivity and high thermoelectric figure of merit in *n*-type $Ba_xYb_yCo_4Sb_{12}$ double-filled skutterudites, Appl. Phys. Lett. **92**, 182101 (2008).

[18] T. Dahal, Q. Jie, G. Joshi, S. Chen, C. F. Guo, Y. C. Lan, and Z. F. Ren, Thermoelectric property enhancement in Yb-doped *n*-type skutterudites $Yb_xCo_4Sb_{12}$, Acta Mater. **75**, 316 (2014).

[19] Y. Tang, S.-W. Chen, and G. J. Snyder, Temperature dependent solubility of Yb in Yb-$CoSb_3$ skutterudite and its effect on preparation, optimization and lifetime of thermoelectrics, J. Materiomics **1**, 75 (2015).

[20] Y. L. Tang, R. Hanus, S. W. Chen, and G. J. Snyder, Solubility design leading to high figure of merit in low-cost Ce-$CoSb_3$ skutterudites, Nat. Commun. **6**, 7584 (2015).

[21] S. Y. Wang, J. R Salvador, J. Yang, P. Wei, B. Duan, and J. H. Yang, High-performance *n*-type $Yb_xCo_4Sb_{12}$: From partially filled skutterudites towards composite thermoelectrics, NPG Asia Mater. **8**, e285 (2016).

[22] X. Shi, S. Q. Bai, L. L. Xi, J. Yang, W. Q. Zhang, L. D. Chen, and J. H. Yang, Realization of high thermoelectric performance in *n*-type partially filled skutterudites, J. Mater. Res. **26**, 1745 (2011).

[23] X. Shi, J. Yang, J. R. Salvador, M. F. Chi, J. Y. Cho, H. Wang, S. Q. Bai, J. H. Yang, W. Q. Zhang, and L. D. Chen, Multiple-filled Skutterudites: High thermoelectric figure of merit through separately optimizing electrical and thermal transports, J. Am. Chem. Soc. **133**, 7837 (2011).

[24] V. Keppens, D. Mandrus, B. C. Sales, B. C. Chakoumakos, P. Dai, R. Coldea, M. B. Maple, D. A. Gajewski, E. J. Freeman, and S. Bennington, Localized vibrational modes in metallic solids, Nature (London) **395**, 876 (1998).

[25] M. M. Koza, M. R. Johnson, R. Viennois, H. Mutka, L. Girard, and D. Ravot, Breakdown of phonon glass paradigm in La- and Ce-filled Fe_4Sb_{12} skutterudites, Nat. Mater. **7**, 805 (2008).

[26] I. K. Dimitrov, M. E. Manley, S. M. Shapiro, J. Yang, W. Zhang, L. D. Chen, Q. Jie, G. Ehlers, A. Podlesnyak, J. Camacho, and Q. Li, Einstein modes in the phonon density of states of the single-filled skutterudite $Yb_{0.2}Co_4Sb_{12}$, Phys. Rev. B **82**, 174301 (2010).

[27] C. Chang and L. D. Zhao, Anharmoncity and low thermal conductivity in thermoelectrics, Mater. Today Phys. **4**, 50 (2018).

[28] H. J. Pang, L. C. Cheng, H. Yu, P. F. Qiu, G. H. Zhong, Q. Peng, and X. J. Chen, Hybridization-driven strong anharmonicity in Yb-filled skutterudites, Phys. Rev. B **105**, 094115 (2022).

[29] D. J. Singh and W. E. Pickett, Skutterudite antimonides: Quasi-linear bands and unusual transport, Phys. Rev. B **50**, 11235 (1994).

[30] T. Caillat, A. Borshchevsky, and J.-P. Fleurial, Properties of single crystalline semiconducting $CoSb_3$, J. Appl. Phys. **80**, 4442 (1996).

[31] J. O. Sofo and G. D. Mahan, Electronic structure of $CoSb_3$: A narrow-band-gap semiconductor, Phys. Rev. B **58**, 15620 (1998).

[32] H. Anno, K. Matsubara, Y. Notohara, T. Sakakibara, and H. Tashiro, Effects of doping on the transport properties of $CoSb_3$, J. Appl. Phys. **86**, 3780 (1999).

[33] J. S. Dyck, W. Chen, C. Uher, L. D. Chen, X. F. Tang, and T. Hirai, Thermoelectric properties of the n-type filled skutterudite $Ba_{0.3}Co_4Sb_{12}$ doped with Ni, J. Appl. Phys. **91**, 3698 (2002).

[34] J. R. Salvador, J. Yang, H. Wang, and X. Shi, Double-filled skutterudites of the type $Yb_xCa_yCo_4Sb_{12}$: Synthesis and properties, J. Appl. Phys. **107**, 043705 (2010).

[35] V. L. Kuznetsov, L. A. Kuznetsova, and D. M. Rowe, Effect of partial void filling on the transport properties of $Nd_xCo_4Sb_{12}$ skutterudites, J. Phys.: Condens. Matter **15**, 5035 (2003).

[36] E. B. Isaacs and C. Wolverton, Electronic structure and phase stability of Yb-filled $CoSb_3$ skutterudite thermoelectrics from first-principles, Chem. Mater. **31**, 6154 (2019).

[37] J. C. Smith, S. Banerjee, V. Pardo, and W. E. Pickett, Dirac Point Degenerate with Massive Bands at a Topological Quantum Critical Point, Phys. Rev. Lett. **106**, 056401 (2011).

[38] V. Pardo, J. C. Smith, and W. E. Pickett, Linear bands, zero-momentum Weyl semimetal, and topological transition in skutterudite-structure pnictides, Phys. Rev. B **85**, 214531 (2012).

[39] E. Arushanov, M. Respaud, and T. Caillat, Shubnikov-de Haas oscillations in $CoSb_3$ single crystals, Phys. Rev. B **61**, 4672 (2000).

[40] M. Naumann, P. Mokhtari, Z. Medvecka, F. Arnold, M. Pillaca, S. Flipo, D. Sun, H. Rosner, A. Leithe-Jasper, P. Gille, M. Baenitz, and E. Hassinger, Fermi surface of the skutterudite $CoSb_3$: Quantum oscillations and band-structure calculations, Phys. Rev. B **103**, 085133 (2021).

[41] B. H. Yan, L. Müchler, X. L. Qi, S. C. Zhang, and C. Felser, Topological insulators in filled skutterudites, Phys. Rev. B **85**, 165125 (2012).

[42] Y. L. Li, P. F. Qiu, Z. Xiong, J. K. Chen, R. Nunna, X. Shi, and L. D. Chen, Electrical and thermal transport properties of $Yb_xCo_4Sb_{12}$ filled skutterudites with ultrahigh carrier concentrations, AIP Adv. **5**, 117239 (2015).

[43] G. Kresse and J. Joubert, From ultrasoft pseudopotentials to the projector augmented-wave method, Phys. Rev. B **59**, 1758 (1999).

[44] G. Kresse and J. Furthmüller, Efficient iterative schemes for *ab initio* total-energy calculations using a plane-wave basis set, Phys. Rev. B **54**, 11169 (1996).

[45] J. P. Perdew, K. Burke, and M. Ernzerhof, Generalized Gradient Approximation Made Simple, Phys. Rev. Lett. **77**, 3865 (1996).

[46] I. Souza, N. Marzari, and D. Vanderbilt, Maximally localized Wannier functions for entangled energy bands, Phys. Rev. B **65**, 035109 (2001).

[47] Q. S. Wu, S. N. Zhang, H. F. Song, M. Troyer, and A. A. Soluyanov, WannierTools: An open-source software package for novel topological materials, Comput. Phys. Commun. **224**, 405 (2018).

[48] T. M. Tritt (ed.), *Recent Trends in Thermoelectric Materials Research* (Academic, San Diego, 2001).

[49] W. Jeitschko and D. Braun, $LaFe_4P_{12}$ with filled $CoAs_3$-type structure and isotypic lanthanoidtransition metal polyphosphides., Acta Cryst. B **33**, 3401 (1977).

[50] B. C. Sales, B. C. Chakoumakos, and D. Mandrus, Thermoelectric properties of thallium-filled skutterudites, Phys. Rev. B **61**, 2475 (2000).

[51] N. R. Dilley, E. D. Bauer, M. B. Maple, and B. C. Sales, Thermoelectric properties of chemically substituted skutterudites $Yb_yCo_4Sn_xSb_{12-x}$, J. Appl. Phys. **88**, 1948 (2000).

[52] L. D. Chen, T. Kawahara, X. F. Tang, T. Goto, T. Hirai, J. S. Dyck, W. Chen, and C. Uher, Anomalous barium filling fraction and n-type thermoelectric performance of $Ba_yCo_4Sb_{12}$, J. Appl. Phys. **90**, 1864 (2001).

[53] B. L. Huang and M. Kaviany, Filler-reduced phonon conductivity of thermoelectric skutterudites: *Ab initio* calculations and molecular dynamics simulations, Acta Mater. **58**, 4516 (2010).

[54] C. Uher, Recent trends in thermoelectric materials research I, Semiconductors and Semimetals. **69**, 139 (2001).

[55] B. C. Sales, D. Mandrus, B. C. Chakoumakos, V. Keppens, and J. R. Thompson, Filled skutterudite antimonides: Electron crystals and phonon glasses, Phys. Rev. B **56**, 15081 (1997).

[56] D. Wee, B. Kozinsky, N. Marzari, and M. Fornari, Effects of filling in $CoSb_3$: Local structure, band gap, and phonons from first principles, Phys. Rev. B **81**, 045204 (2010).

[57] E. O. Kane, Band structure of indium antimonide, J. Phys. Chem. Solids **1**, 249 (1957).

[58] H. J. Goldsmid, *Thermoelectric Refrigeration* (Plenum, New York, 1964).

[59] L. Chaput, P. Pécheur, J. Tobola, and H. Scherrer, Transport in doped skutterudites: *Ab initio* electronic structure calculations, Phys. Rev. B **72**, 085126 (2005).

[60] Y. Z. Pei, A. D. LaLonde, H. Wang, and G. J. Snyder, Low effective mass leading to high thermoelectric performance, Energy Environ. Sci. **5**, 7963 (2012).

[61] G. J. Snyder, A. H. Snyder, M. Wood, R. Gurunathan, B. H. Snyder, and C. Niu, Weighted mobility, Adv. Mater. **32**, 2001537 (2020).

[62] L. Fu and C. L. Kane, Topological insulators with inversion symmetry, Phys. Rev. B **76**, 045302 (2007).

[63] B. Q. Lv, T. Qian, and H. Ding, Experimental perspective on three-dimensional topological semimetals, Rev. Mod. Phys. **93**, 025002 (2021).

[64] A. A. Abrikosov, Quantum magnetoresistance, Phys. Rev. B **58**, 2788 (1998).

[65] A. A. Abrikosov, Quantum linear magnetoresistance, Europhys. Lett. **49**, 789 (2000).

[66] S. Singh, R. K. Gopal, J. Sarkar, and C. Mitra, Quantum and classical contributions to linear magnetoresistance in topological insulator thin films, AIP Conf. Proc. **1728**, 020557 (2016).

[67] H. Zhang, J. Nichols, and J. W. Brill, Weak localization of bulk channels in topological insulator thin films, Phys. Rev. B **84**, 125134 (2011).

[68] Y. F. Lee, S. Punugupati, F. Wu, Z. Jin, J. Narayan, J. Schwartz, Evidence for topological surface states in epitaxial Bi$_2$Se$_3$ thin film grown by pulsed laser deposition through magneto-transport measurements, Curr. Opin. Solid State Mater. Sci. **18**, 279 (2014).

[69] A. Nivedan, K. Das, S. Kumar, A. Singh, S. Mardanya, A. Agarwal, and S. Kumar, Magnetic field-dependent resistance crossover and anomalous magnetoresistance in topological insulator Bi$_2$Te$_3$, J. Phys.: Condens. Matter **32**, 425002 (2020).

[70] D. Mandrus, A. Migliori, T. W. Darling, M. F. Hundley, E. J. Peterson, and J. D. Thompson, Electronic transport in lightly doped CoSb$_3$, Phys. Rev. B **52**, 4926 (1995).

[71] G. J. Snyder, A. Pereyra, and R. Gurunathan, Effective mass from Seebeck coefficient, Adv. Funct. Mater. **32**, 2112772 (2022).

[72] W. Zawadzki, Electron transport phenomena in small-gap semiconductors, Adv. Phys. **23**, 435 (1974).